2014/2500M-0011

ISSN 1797-3457 (verkkojulkaisu)
ISBN (PDF) 978-951-25-2636-9

TIIVISTELMÄRAPORTTI (SUMMARY REPORT)

Military communication using orbital angular momentum based radio (MORAMBA2)

Tutkimuksen johtaja: Professori Aarne Mämmelä, aarne.mammela@vtt.fi
Tutkijat: Tommi Dufva, Adrian Kotelba, Johan Sten
VTT Technical Research Centre of Finland, Kaitoväylä 1, FI-90571 Oulu

Abstract
The major weakness of any wireless communication system is the ease of intercepting or jamming radio signals, which increases the risk of using or altering radio signals by unauthorized persons or prevents the usability of a communication system. The possibility of creating secure communications links impervious to threats and external attacks by exploiting light orbital angular momentum (OAM) has already been recognized by Defense Advanced Research Projects Agency. In this work, we study possibility of creating secure links using OAM-based radio transmission. We analyze the process of generating and receiving OAM wave modes by using the theory of spherical wave functions with special emphasis on antenna location perturbations. We also develop methods to transmit and receive OAM wave modes by using phase mode excitation in circular antenna arrays. We demonstrate that mutual orthogonality of OAM wave modes is extremely sensitive to misalignments of the transmitter and/or the receiver and multipath propagation which can be exploited to set up point-to-point secure radio links.

1. Introduction

The broadcast nature of the wireless communication medium makes it hard to eliminate unauthorized access to wireless networks. For that reason, it is relatively easy to eavesdrop on wireless interfaces in general. Moreover, in wireless networks, the risk of using or altering radio signals by unauthorized persons or preventing the usability of a communication system is significantly higher than in wired networks. In conventional military communication systems, the protection of own information is usually achieved by obscuring the information transmission using cryptography, special modulation schemes such as spread-spectrum modulation, or both.

Transmissions techniques using so-called light orbital angular momentum wave modes were studied in detail in [Allen et al. 1992] and are rather well established, both in free-space and fibre optical communications. Generation, transformation, and measurement of the orbital angular momentum of millimeter-wave were studied in [Brand 1998] and WiFi band in [Mohammadi et al. 2010]. In scientific literature, operation of radio links using OAM wave modes have been reported at the frequencies of 2.4 GHz, 10 GHz, 17 GHz, 29 GHz, 60 GHz, and 100 GHz over distances up to 440 m.

The possibility of creating highly secure communications links impervious to threats and external attacks by exploiting light orbital angular momentum (OAM) has already been recognized by Defense Advanced Research Projects Agency (DARPA). In 2011, DARPA funded research efforts related to secure communication using optical vortices. The researchers were to investigate the properties of light beams carrying OAM in optical fibers and their applicability to creating next generation secure encryption links, by encoding information in different OAM states.

In [Linturi et al. 2013], OAM-based transmission in radio frequency bands has recently been recognized as one of the 100 most important future technologies for Finland.

2. Research objectives and accomplishment plan

In this work, we study the applicability of the transmission technique that exploits orbital angular momentum (OAM) state of a radio beam to securely transmit information in wireless military systems. The main objectives of this research are: 1) to exploit the characteristics of signals transmitted using OAM-based radio techniques and identify the military communication systems, where OAM-based radio techniques can be implemented, 2) to examine possible limitations of the theory of OAM-based radio transmission suggested by the theory based on spherical wave functions, 3) to carry out theoretical and simulation based performance evaluation of OAM-based radio wave generation and reception techniques, taking into account realistic radio-electrical environments and relevant propagation parameters. Develop suitable algorithms, 4) demonstrate by simulations the jamming resilience and difficulty of intercepting the signal transmitted with selected OAM-based radio techniques.

In the first phase, executed in the year 2013, the general properties of OAM-carrying radio beams were studied. In the second phase, executed in the year 2014, new radio transmission schemes were developed. In almost all publicly reported experiments with OAM wave modes, a specially crafted parabolic antenna, also known as spiral-phase-plate antenna, was used. In this work, we develop alternative ways to generate and receive radio beams carrying OAM using circular antenna arrays. New signal processing algorithms for controlling antenna arrays are developed.

Finally, in the third phase to be executed in the year 2015, the high-level algorithm simulations will be made in MATLAB and commercial electromagnetic field simulation software. Visualization tools will be developed to help to understand the properties of the radio beams carrying OAM as well as generation, reception, detection, and interception of those radio beams.

3. Materials and methods

3.1. Overview

Two different methods were used in the analysis. The first method is based on the theory of spherical wave functions and the singular value decomposition. The second method is based on numerical electromagnetic simulations by using an in-house integral equation solver. These two methods are shortly described in the reminder of this Section.

3.2. Free-space radio link explained by spherical wave functions

Consider a free-space radio link consisting of a transmitter and a receiver as shown in Fig. 1. The electromagnetic field $\mathbf{E}$ radiated by the transmitter can be expressed by an expansion

$$\mathbf{E}(\omega,\mathbf{r}) = \sqrt{\eta}\frac{i\omega}{c}\sum_{l=1}^{N^{\mathrm{tx}}}\sum_{m=-l}^{l}\sum_{n=2}^{3} a_{l,m,n}(\omega)\Psi_{l,m,n}^{\mathrm{out}}\left(\frac{\omega\mathbf{r}}{c}\right)$$

where ω is the angular frequency of oscillation, $\mathbf{r}$ is a position in space, η is the wave impedance in free-space, c is the speed of light, $a_{l,m,n}$ are expansion coefficients, $\Psi_{l,m,n}^{\mathrm{out}}$ are outgoing spherical vector wave functions, and N^{tx} is the highest order of the wave functions in the expansion. The same field in the vicinity of the receiver can be expressed by an expansion

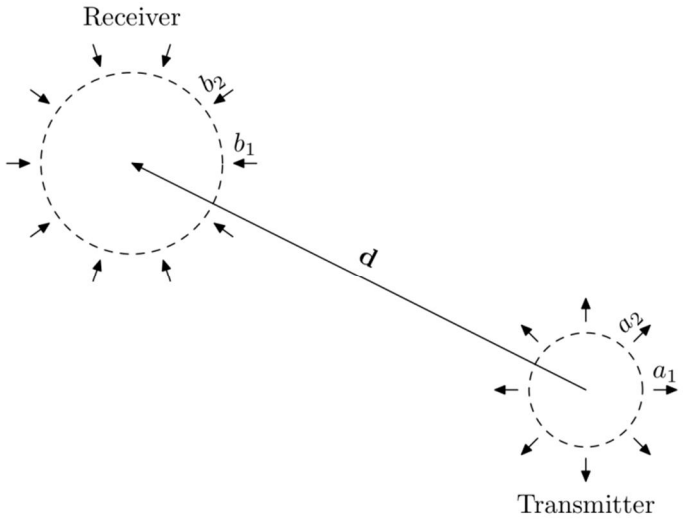

Figure 1. Free-space radio link described by spherical wave functions.

$$\mathbf{E}(\omega, \mathbf{d}+\mathbf{r}) = \sqrt{\eta}\frac{i\omega}{c}\sum_{l=1}^{N^{\mathrm{rx}}}\sum_{m=-l}^{l}\sum_{n=2}^{3} b_{l,m,n}(\omega)\Psi_{l,m,n}^{\mathrm{reg}}\left(\frac{\omega\mathbf{r}}{c}\right)$$

where $\mathbf{d}$ is a vector from the transmitter to the receiver, $b_{l,m,n}$ are expansion coefficients, $\Psi_{l,m,n}^{\mathrm{reg}}$ are regular spherical vector wave functions, and N^{rx} is the highest order of the wave functions in the expansion. The above vector spherical wave functions are formulated as

$$\Psi_{l,m,2}\left(\frac{\omega\mathbf{r}}{c}\right) = \frac{1}{\sqrt{2\pi}}\frac{1}{\sqrt{l(l+1)}} z_l\left(\frac{\omega r}{c}\right)\left[-\hat{\theta}\frac{m\bar{P}_l^m(\cos\theta)}{\sin\theta} - i\hat{\phi}\frac{d\bar{P}_l^m(\cos\theta)}{d\theta}\right]\exp(im\phi)$$

$$\Psi_{l,m,3}\left(\frac{\omega\mathbf{r}}{c}\right) = \frac{1}{\sqrt{2\pi}}\frac{1}{\sqrt{l(l+1)}}\left\{l(l+1)\frac{c}{\omega r} z_l\left(\frac{\omega r}{c}\right)\hat{r}\bar{P}_l^m(\cos\theta) + \left[z_l'\left(\frac{\omega r}{c}\right) + \frac{c}{\omega r} z_l\left(\frac{\omega r}{c}\right)\right]\left[\hat{\theta}\frac{d\bar{P}_l^m(\cos\theta)}{d\theta} + i\hat{\phi}\frac{m\bar{P}_l^m(\cos\theta)}{\sin\theta}\right]\right\}\exp(im\phi)$$

where z_l is a spherical Hankel or Bessel function, depending on the type of the wave function, and $\bar{P}_l^m$ is a normalised Legendre function.

The expansion coefficients are related as

$$b = Ta$$

where a is a vector consisting of the expansion coefficients a_j, b is a vector consisting of the expansion coefficients b_j, and T is called a translation matrix. Matrix T serves also as a channel matrix for the spherical wave modes from the transmitter to the receiver.

As any matrix, T has a singular value decomposition

$$T = U\Sigma V^*$$

where U and V are unitary matrices and Σ is a diagonal matrix. The singular value decomposition arranges T in orthogonal channels:

$$b = Ub', \quad b' = \Sigma a', \quad a' = V^* a.$$

Above, each column of V gives expansion coefficients for the radiation mode of one orthogonal channel. Similarly, each column of U gives expansion coefficients for the reception

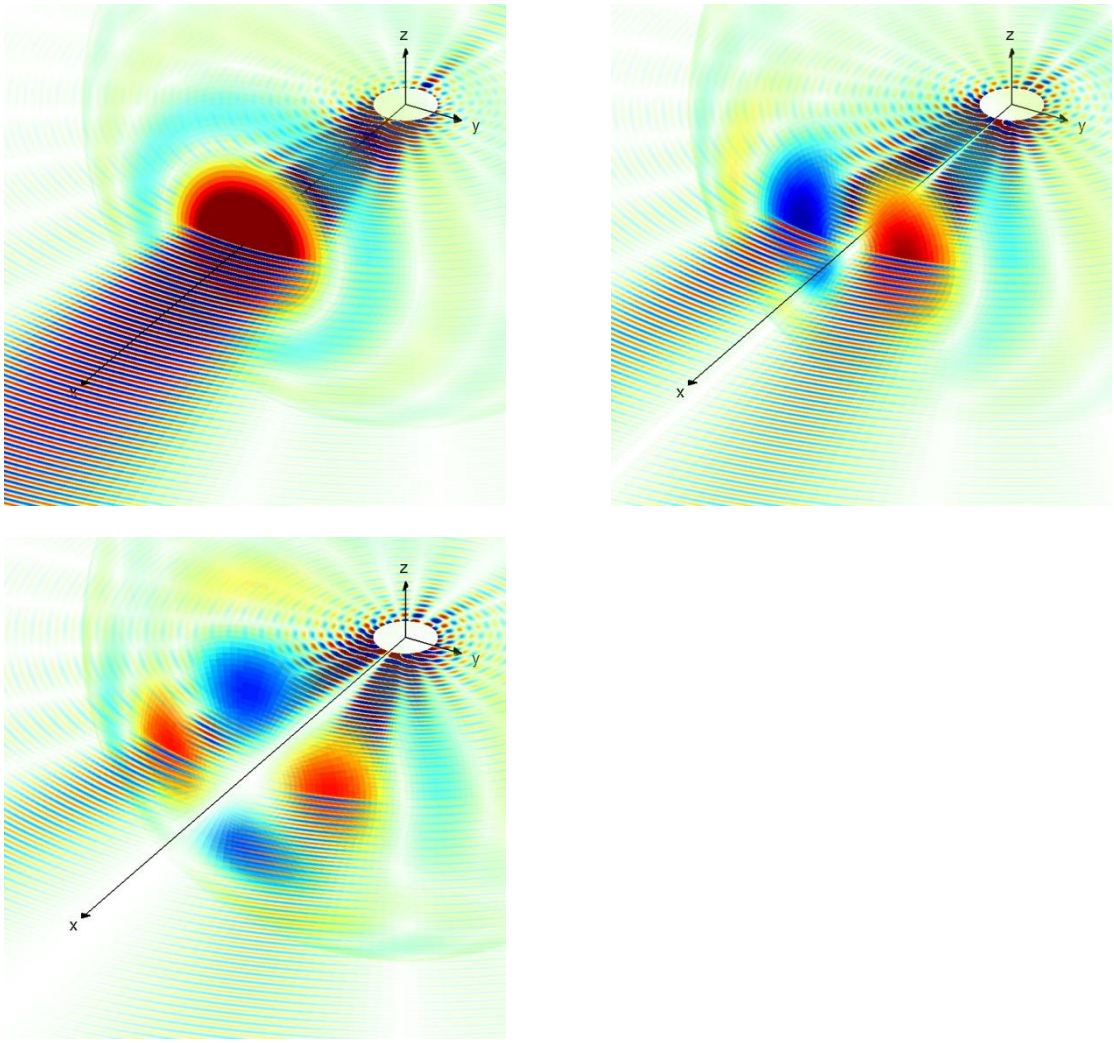

Figure 2. Radiation modes of the first ten orthogonal channels: one of the modes 1–2 in the upper-left plot, one of the modes 3–6 in the upper-right plot, and one of the modes 7–10 in the lower-left plot.

mode of one orthogonal channel.

The diagonal entries of Σ give the gains of the channels. By the definition of the singular value decomposition, the channels are arranged in the order of decreasing gain.

The three plots in Fig. 2 illustrate the radiation modes of the first ten orthogonal channels. The upper-left plot presents one of the modes 1–2. These modes correspond to the radiation of a typical radio transmitter with a maximal directivity in the direction of the receiver (here in the direction of the x-axis). The two different modes correspond to the two different polarisations. The upper-right plot presents one of the modes 3–6. These modes correspond to the so-called OAM modes of order $m=1$. The four different modes correspond to the two different polarisations times the two different handedness of rotation. There is a phase singularity and an amplitude zero of order $m=1$ in the direction of the receiver. The lower-left plot presents one of the modes 7–10. These modes correspond to the OAM modes of order $m=2$. The four different modes correspond to the two different polarisations times the two different handedness of rotation. There is a phase singularity and an amplitude zero of order $m=2$ in the direction of the receiver.

Table 1. Theoretical path loss in dB as a function of the link distance

$\log(d/\lambda)$ / Channels	2.5	3.0	3.5	4.0	4.5	5.0	5.5
1-2	0.0	3.3	12.1	22.0	32.0	42.0	52.0
3-6	0.3	11.2	30.1	50.0	70.0	90.0	110.0
7-10	1.5	22.5	51.6	81.5	111.5	141.5	171.5

Table 2. Theoretical path loss in dB as a function of the transmitter and receiver sizes

L/λ / Channels	5.6	10.0	17.8	31.6	56.2	100.0	177.8
1-2	50.9	41.8	31.8	22.0	12.1	3.3	0.0
3-6	107.7	89.6	69.5	50.0	30.1	11.3	0.3
7-10	168.1	140.9	110.8	81.5	51.6	22.7	1.5

The aforementioned method does not make any assumptions on the transmitter and the receiver other than their sizes. The method provides theoretical bounds for free-space radio.

3.3. Numerical electromagnetic simulations

Let us consider the antenna structure that consists of three concentric circular antenna arrays. The first, innermost, array consists of just one antenna element in the center of the structure. The second, middle, array consists of four antenna elements on a circle with radius of $45\,\lambda$. The third, outermost, array consists of eight antenna elements on a circle with radius of $50\,\lambda$. The symbol $\lambda = 2\pi c/\omega$ denotes the wavelength. Each of the three arrays is driven through a separate feeding network consisting of phase shifters and Wilkinson power dividers. The sizes of the arrays are adjusted so that the strengths of the channels are approximately equal when the link distance is $10\,000\,\lambda$. The communication direction is in the direction of the x-axis. The structure uses identical antenna elements. Each antenna element is a Yagi-antenna that consists of six dipoles: a reflector, a driven dipole and four directors. The length of the Yagi-antenna is $1.38\,\lambda$. The directivity of the Yagi-antenna is approximately 9.8 dB.

A free-space radio link using the above antenna structure in both the transmitter and the receiver was analysed by using an in-house electromagnetic integral equation solver. The results of the analysis are presented in Sec. 4.2.

4. Results and discussion

4.1. Theoretical results for a free-space radio link by using spherical wave functions

The first example considers the theoretical path loss as a function of the link distance. In the example, the approximate diameters of the transmitter and the receiver are both $32\,\lambda$, and the link distance d varies from $316\,\lambda$ to $316\,228\,\lambda$. The results are presented in Tab. 1. It can be seen that as d gets tenfold, the channels 1–2 decay 20 dB, the channels 3–6 decay 40 dB, and the channels 7–10 decay 60 dB.

The second example considers the theoretical path loss as a function of the transmitter and receiver sizes. In the example, the link distance is $10\,000\,\lambda$, and the approximative diameters of the transmitter and the receiver are both equal to L varying from $6\,\lambda$ to $178\,\lambda$. The results are presented in Tab. 2. It can be seen that as L is grown by the factor of $\sqrt{10} \approx 3.16$, the channels 1–2 strengthen 20 dB, the channels 3–6 strengthen 40 dB, and the channels 7–10 strengthen 60 dB. The square root in the factor is due to the fact that the sizes of both the

Table 3. Channel matrix, when translational misalignment is 20 λ

rx \ tx	1	2	3	4	5	6	7	8	9	10
1	-50.9		-62.5	-62.5	-59.5					
2		-50.9	-62.5	-62.5		-59.5				
3	-62.5	-62.5	-50.0				-59.9	-59.9		
4	-62.5	-62.5		-50.0			-59.9	-59.9		
5	-59.5				-50.1				-56.9	
6		-59.5				-50.1				-56.9
7			-59.9	-59.9			-51.8			
8			-59.9	-59.9				-51.8		
9					-56.9				-51.8	
10						-56.9				-51.8

Table 4. Channel matrix, when translational misalignment is 40 λ

rx \ tx	1	2	3	4	5	6	7	8	9	10
1	-50.9		-56.5	-56.5	-53.5			-60.4	-60.4	
2		-50.9	-56.5	-56.5		-53.5	-60.4			-60.4
3	-56.5	-56.5	-49.4		-59.2	-59.2	-54.1	-54.1	-66.1	-66.1
4	-56.5	-56.5		-49.4	-59.2	-59.2	-54.1	-54.1	-66.1	-66.1
5	-53.5		-59.2	-59.2	-49.4			-63.1	-51.1	
6		-53.5	-59.2	-59.2		-49.4	-63.1			-55.1
7		-60.4	-54.1	-54.1		-63.1	-50.4			
8	-60.4		-54.1	-54.1	-63.1			-50.4		
9	-60.4		-66.1	-66.1	-51.1				-50.4	
10		-60.4	-66.1	-66.1		-51.1				-50.4

transmitter and the receiver are changing.

The third example considers the sensitivity of the channel orthogonality to the translational misalignment of the receiver. In the example, the link distance is 10 000 λ, and the approximative diameters of the transmitter and the receiver are equal but vary with channels: 6 λ for Ch 1–2, 32 λ for Ch 3–6, 56 λ for Ch 7–10. This was done in order to have the strengths of the ten different channels approximatively equal. The channel matrix was computed for three different translational misalignments of the receiver: 0 λ, 20 λ, and 40 λ. When the misalignment is 0 λ, the channel matrix is perfectly orthogonal. For that reason, it is not shown here. The other results are presented in Tabs. 3–4. Only the values over -70 dB are shown. The following observations can be made: When the misalignment is 20 λ, there appear cross-talking between the channels, which in its worst is approximately 6 dB below the signal. When the misalignment is 40 λ, the orthogonality is lost completely.

The sensitivity of the channel orthogonality to the rotational misalignment of the receiver was also studied. The channel matrix was computed for three different rotational misalignments of the receiver: 0°, 0.1°, and 0.2°. Due to the page limitation, the numerical results are not shown here. However, the following observations were made: When the misalignment is 0°, the channel matrix is perfectly orthogonal. When the misalignment is 0.1°, there appear cross-talking between the channels, which in its worst is approximately 8 dB below the signal. When the misalignment is 0.2°, the orthogonality is lost completely.

4.2. Computed results for a free-space radio link by using electromagnetic simulations

Table 5. Computed path loss in dB as a function of the link distance

$\log(d/\lambda)$ / Channels	2.5	3.0	3.5	4.0	4.5	5.0	5.5
1	52.2	62.2	72.2	82.3	92.3	102.3	112.3
3 and 5	53.3	80.0	74.5	82.6	100.4	120.1	140.1
7 and 9	52.8	56.3	74.7	82.2	110.6	140.6	170.4

This section presents computed results for a free-space radio link when both the transmitter and the receiver use the antenna structure explained in Sec. 3.2.

In the following example, the path loss was computed in cases where the link distance d varies from $316\,\lambda$ to $316\,228\,\lambda$. The results are presented in Tab. 5. It can be seen that the path loss behaves similarly as in the theoretical results in Tab. 1, only the overall strengths of the channels are much lower. This is because in this example the radio link is setup by using specific antenna structures, which are not ideal.

The sensitivity of the channel orthogonality to the translational and the rotational misalignment was analysed in a similar manner as in Sec. 4.1. Due to the page limitation, the numerical results are not shown here. However, it is noted that the results were similar to those presented in Sec. 4.1.

In general, the results obtained by the two very different methods explained in Secs. 3.2. and 3.3. and presented in Secs. 4.1. and 4.2. show very similar behaviour of a free-space radio link using the so-called OAM modes.

4.3 Generation of higher-order modes with circular antenna arrays

The far-field radiation pattern of any antenna array is determined by the amplitude and phase weighting of each individual element. This weighting function is commonly referred to as the array excitation function. For circular antenna arrays, the array excitation function $F(\vartheta)$ is necessarily periodic with period 2π radians due to array geometry, that is,

$$F(\vartheta) = \sum_{m=-M}^{M} F_m(\vartheta) = \sum_{m=-M}^{M} w_m \exp(im\vartheta)$$

where w_m represents the complex Fourier coefficient of the mth spatial harmonic of the array excitation function. Each of the $(2M+1)$ terms of $F(\vartheta)$ is commonly called a phase mode excitation of the array.

For a continuous circular array with a radius R, the far-field directional pattern $D_m(\theta,\phi)$ arising from the mth phase mode has a similar phase variation with azimuthal angle as the array excitation function but amplitude scaled by a Bessel function coefficient. In particular,

$$D_m(\theta,\phi) = \int_0^{2\pi} w_m \exp[ikR\sin\theta\cos(\phi-\vartheta) + im\vartheta]\,d\vartheta = 2\pi R w_m i^m J_m(kR\sin\theta)\exp(im\phi)$$

where θ denotes polar angle, φ is azimuthal angle, and $J_m(x)$ denotes the mth order Bessel function of the first kind. Note that directional pattern exhibits similar azimuthal phase behaviour as the regular spherical vector wave functions presented in Sec. 3.2.

Since $k = 2\pi/\lambda$, in order to determine how many phase modes can be excited for a continuous circular array of radius R, one needs to study the behaviour of the Bessel functions $J_m(kR\sin\theta)$. By studying the plots of a few first low-order Bessel functions, we can conclude that OAM mode with reasonable strength is obtained when the order of the mode m is comparable to the argument of the Bessel functions. In other words, the continuous circular array with a radius R is expected to generate OAM modes with reasonable strength

up to order $M \approx 2\pi R/\lambda$.

For a more practical, *N*-element array with equal spacing between elements, we sample the continuous array around the circumference. Thus, *N* radiating elements are located at angles $\vartheta_n = 2\pi n/N$ where n=0,1,…,N-1. If a continuous circular array generates *M* spatial harmonics, then, according to spatial version of sampling theorem, we need at least (2*M*+1) elements to reproduce those spatial harmonics, which implies that the spacing between adjacent elements on the arc cannot exceed half-wavelength.

Multiplexing of many OAM modes is relatively straightforward provided that antenna array is able to excite the corresponding phase modes. Let us assume that we want to transmit complex symbols $X_{-M},\dots,X_0,\dots,X_M$. For example, one can simply define excitation weights as

$$w_m = \frac{1}{2\pi i^m J_m(kR)} X_m$$

for all $m = -M,\dots,0,\dots M$. This weighting causes all of the modes to contribute equally to the beam pattern. Consequently, the signal to be sent from the *n*th transmit element of an *N*-element circular antenna array is

$$s_n = \frac{1}{2\pi}\sum_{m=-M}^{M} \frac{\exp(im\vartheta_n)}{i^m J_m(kR)} X_m = \frac{1}{2\pi}\sum_{m=-M}^{M} \frac{\exp(2\pi imn/N)}{i^m J_m(kR)} X_m$$

which can be efficiently implemented using linear pre-processing and Inverse Discrete Fourier Transform matrices.

4.4 Reception of higher-order modes with circular antenna arrays

Let us consider a continuous circular array with a radius R located in xy plane and assume that the OAM-carrying beam arrives from direction described by polar angle θ and azimuthal angle ϕ. The array response to the incoming signal is

$$r = \sum_{m=-M}^{M} \int_0^{2\pi} w(\vartheta) X_m \exp[ikR\sin\theta\cos(\phi-\vartheta) + im\psi]\, d\vartheta$$

where

$$\psi = \tan^{-1}\left(\frac{y_0 + R\sin\vartheta}{x_0 + R\cos\vartheta}\right)$$

is the phase of the incoming beam at misaligned location of the reception array (x_0, y_0). The lth phase modes can be extracted from the signal r without any crosstalk provided that the mode excitation function of the reception array $w_l(\vartheta)$ is made orthogonal to $\exp[ikR\sin\theta\cos(\varphi-\vartheta) + im\psi]$ for all $m \neq l$. Thus, transmitted symbols can be extracted from the signal r without any crosstalk by passing the signal *r* through a parallel bank of (2*M*+1) crosscorrelators provided that array excitation functions $w_l(\vartheta)$, $l = -M,\dots,0,\dots M$, form a set of orthonormal basis functions, that is, the crosscorrelation coefficient

$$\varrho_{lm} = \int_0^{2\pi} w_l(\vartheta) w_m^*(\vartheta) d\vartheta = \begin{cases} 0 & l \neq m \\ 1 & l = m \end{cases}$$

where asterisk denotes complex conjugation. The simplest set of orthonormal functions is

$$w_l(\vartheta) = \exp[-ikR\sin\theta\cos(\varphi-\vartheta) - il\psi]$$

which requires perfect knowledge of direction of arrival (θ,ϕ). Due to space limitations, we do not present the plots of crosscorrelation coefficients for different antenna misalignments but mention one interesting case. Namely, when total displacement $x_0^2 + y_0^2 < R^2$, then for even values of $|m-l|$, the crosscorrelation ϱ_{lm} is zero. In other words, when direction of arrival (θ,ϕ) and antenna location (x_0, y_0) are perfectly known, $x_0^2 + y_0^2 < R^2$, then the orthogonality between some modes is preserved even with small translational antenna misalignment.

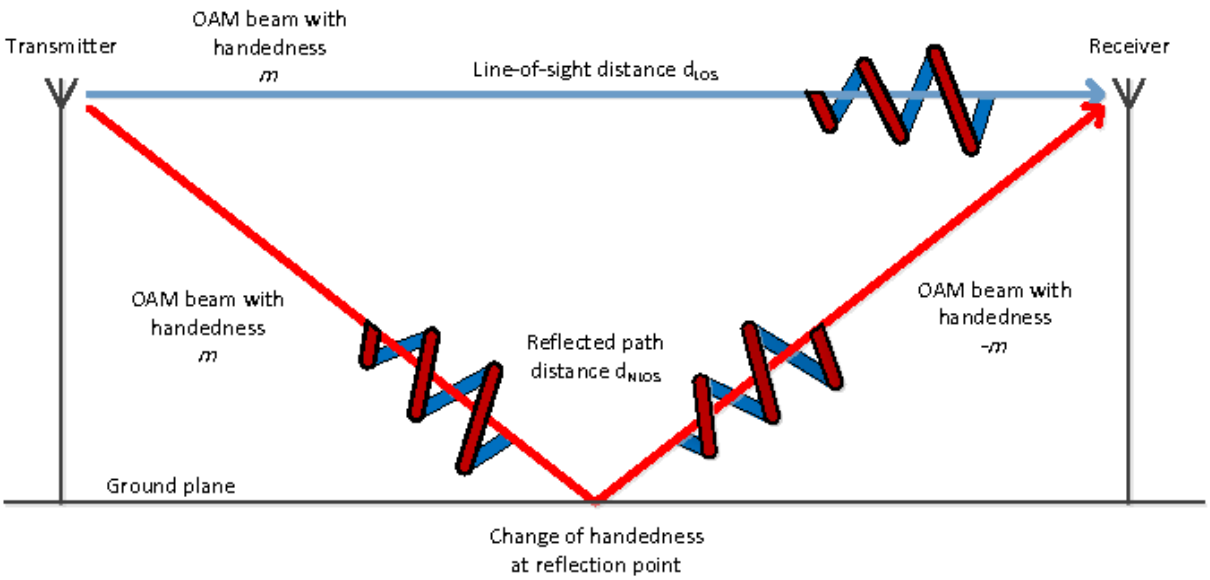

Figure 3. Propagation of OAM wave modes in a two-ray channel.

For a more practical, *N*-element circular arrays with equal spacing between elements, we sample the continuous array around the circumference. Thus, *N* radiating elements are located at angles $\vartheta_n = 2\pi n/N$ where n=0,1,…,N-1 and integration is replaced by summation. The bank of crosscorellators can be efficiently implemented using Discrete Fourier Transform matrices.

4.5 Multipath propagation of OAM wave modes

Let us consider a simple two-ray propagation channel shown in Fig. 3. We assume that the receiver antenna receives two signal components: direct line-of-sight component and a ground-reflected component. These two components arrive at different time instants due to difference in propagation distance and usually are not collinear, which means that their angles-of-arrival are different.

Angular momentum is a cross product of the position vector and linear momentum. Consequently, the angular momentum is an axial vector which means that it changes sign under space reflection. In other words, the handedness of OAM wave mode is reversed when it is reflected off of a surface. Similar effects are observed also for circularly polarized wave modes, the polarization is reversed when the wave is reflected from a surface.

Two-ray propagation channel is a rather simple model. The signal received by receiver is subject to cross-mode interference because the signal reflected from the ground changes its handedness. In a real environment, the number of reflections cannot be controlled. Thus, the signal received by receiver will be subject to cross-mode interference if the number of reflections is odd and same-mode interference if the number of reflections is even.

If the interference is treated as noise, then one observes signal-to-noise degradation at the output of detector. We simulated different interference scenarios for the first order OAM wave modes and found that degradation of signal-to-noise ratio due to cross-mode interference is between 3 and 6 dB. On the other hand, the signal-to-noise degradation due to same-mode interference is essentially unbounded. The worst-case interference is when the phase difference between direct and reflected component is around 180 degrees and both components are collinear or almost collinear.

5. Conclusions

We have demonstrated the existence of so-called OAM wave modes using theory of spherical wave functions and discussed how they can be generated and received with circular antenna arrays. The additional OAM wave modes form a set of additional independent parallel radio channels that can be exploited as additional degrees of freedom by the system designer. For example, they can be used to obscure information transmission by means of mode hopping. Nevertheless, there are certain limitations in using OAM wave modes.

Perhaps one of the most important limitations is relatively fast decay of signal strength with the distance. In particular, while the two basic radio channels using two orthogonal polarizations decay as $1/d^2$, the additional radio channels using the OAM modes decay as $1/(d^{2+2|m|})$ where d is the link distance and m is the order of the OAM mode. This is a direct consequence of the fact that for higher-order OAM wave modes, most of the transmitted energy is concentrated in a ring whose diameter increases with the distance. However, the weakness of the additional radio channels using the OAM modes can be compensated by enlarging the transmitter and/or the receiver antennas which sometimes is not practical.

From signal processing point of view, transmission of OAM modes shares many similarities to multicarrier transmissions. In particular, OAM-based system and multicarrier system are sensitive to phase noise. Furthermore, the orthogonality of OAM wave modes is sensitive to a misalignment of the transmitter and/or the receiver antennas and multipath propagation that for the purpose of current studies can be understood as forms of spatial phase noise. For OAM wave modes, multipath propagation is a more subtle phenomenon because each reflection introduces OAM wave-mode swap from left- to right-handed one and vice versa. To cope with the problem of wave-mode swap, the receiver must be able to discriminate and, possibly, combine left- and right-handed modes, for example, by using a circular array of $2M+1$ antennas.

It seems possible that the sensitivity of the channel orthogonality to a misalignments of the transmitter and/or the receiver and multipath propagation can be exploited to set up point-to-point secure radio links, for example tactical data links for Command, Control, Communications, Computers, and Intelligence (C4I) applications, which would be difficult to intercept and resilient to jamming.

References

[Allen et al. 1992] L. Allen et al., “Orbital angular momentum of light and the transformation of Laguerre-Gaussian laser modes,” *Physical Review*, vol. 45A, pp. 8185-8189, 1992.

[Brand 1998] Brand, G. F., “Millimeter-wave beams with phase singularities,” *IEEE Transactions on Microwave Theory and Techniques*, vol. 46, pp. 948-951, 1998.

[Linturi et al. 2013] R. Linturi, O. Kuusi, and T. Ahlqvist, ”Suomen sata uutta mahdollisuutta: Radikaalit teknologiset ratkaisut,” Eduskunnan tulevaisuusvaliokunnan julkaisu 6/2013

[Mohammadi et al. 2010] S. M. Mohammadi et al., “Orbital angular momentum in radio - A system study,” *IEEE Transactions on Antennas and Propagation*, pp. 565-572, February 2010.